UC San Diego
UC San Diego Previously Published Works

Title

Development of an Open-Source Dataset of Flat-Mounted Images for the Murine Oxygen-Induced Retinopathy Model of Ischemic Retinopathy.

Permalink

https://escholarship.org/uc/item/3gz9n4z9

Journal

Translational Vision Science & Technology, 13(12)

Authors

Marra, Kyle

Chen, Jimmy

Robles-Holmes, Hailey

et al.

Publication Date

2024-12-02

DOI

10.1167/tvst.13.12.4

Data Science

Development of an Open-Source Dataset of Flat-Mounted Images for the Murine Oxygen–Induced Retinopathy Model of Ischemic Retinopathy

Kyle V. Marra[1,2,*], Jimmy S. Chen[1,*], Hailey K. Robles-Holmes[1], Kristine B. Ly[3], Joseph Miller[1], Guoqin Wei[2], Edith Aguilar[2], Felicitas Bucher[4], Yoichi Ideguchi[2], Fritz Gerald P. Kalaw[1], Andrew C. Lin[1], Napoleone Ferrara[1], J. Peter Campbell[5], Martin Friedlander[2], and Eric Nudleman[1]

[1] Shiley Eye Institute, Viterbi Family Department of Ophthalmology, University of California San Diego, San Diego, CA, USA
[2] Molecular Medicine, The Scripps Research Institute, San Diego, CA, USA
[3] College of Optometry, Pacific University, Forest Grove, OR, USA
[4] Eye Center, Medical Center, Faculty of Medicine, University of Freiburg, Freiburg, Germany
[5] Casey Eye Institute, Department of Ophthalmology, Oregon Health & Science University, Portland, OR, USA

Correspondence: Eric Nudleman, Viterbi Family Department of Ophthalmology and Shiley Eye Institute, University of California San Diego, 9415 Campus Point Dr, MC 0946, La Jolla, CA 92093-0946, USA. e-mail: eric.nudleman@gmail.com

Purpose: To describe an open-source dataset of flat-mounted retinal images and vessel segmentations from mice subject to the oxygen-induced retinopathy (OIR) model.

Methods: Flat-mounted retinal images from mice killed at postnatal days 12 (P12), P17, and P25 used in prior OIR studies were compiled. Mice subjected to normoxic conditions were killed at P12, P17, and P25, and their retinas were flat-mounted for imaging. Major blood vessels from the OIR images were manually segmented by four graders (JSC, HKR, KBL, JM), with cross-validation performed to ensure similar grading.

Results: Overall, 1170 images were included in this dataset. Of these images, 111 were of normoxic mice retina, and 1048 were mice subject to OIR. The majority of images from OIR mice were obtained at P17. The 50 images obtained from an external dataset, OIRSeg, did not have age labels. All images were manually segmented and used in the training or testing of a previously published deep learning algorithm.

Conclusions: This is the first open-source dataset of original and segmented flat-mounted retinal images. The dataset has potential applications for expanding the development of generalizable and larger-scale artificial intelligence and analyses for OIR. This dataset is published online and publicly available at dx.doi.org/10.6084/m9.figshare.23690973.

Translational Relevance: This open access dataset serves as a source of raw data for future research involving big data and artificial intelligence research concerning oxygen-induced retinopathy.

Introduction

The murine oxygen-induced retinopathy (OIR) model is the most widely used in vivo model of ischemic retinopathies, such as retinopathy of prematurity (ROP) and diabetic retinopathy.[1,2] The murine retina is incompletely vascularized at birth. In the OIR model, infant mice (pups) are subject to hyperoxic conditions from postnatal day 7 (P7) to P12 during which time pups develop a central area of vaso-obliteration (VO). On P12, mice are removed from hyperoxia and returned to room air. This immediately induces a state of hypoxia that drives the formation of pre-retinal neovascular tufts resulting in a neovascular phase that peaks at P17. Retinal vasculature spontaneously regresses toward normal architecture by P25. The model mimics hallmark features of ROP, including initial vaso-obliteration followed by neovascularization, and thus the outcome measurements classically included the percentage retinal area covered by NV and VO. Based on these outcome metrics, the OIR model has been used to advance therapeutics by testing the capacity of novel anti-angiogenic factors to rescue retinal vasculature[3–9] and also to understand protective mechanisms against ischemic retinopathy.[10–13]

Recently, there has been an interest in automating quantitative methods to assess various metrics of disease severity in OIR mice. Whereas prior studies used semi-automated machine-learning methods to quantify vascular tortuosity[2] and retinal avascular area,[14] these studies were limited by small sample sizes and remaining need for time-consuming manual input. The advent of deep learning (DL) has resulted in more robust, automated methods to quantify NV and VO (OIRSeg),[15] vascular tortuosity,[16] and endothelial tip cell count.[17] Automated calculation of these biomarkers by DL-based algorithms has the potential to increase the efficiency and throughput of assessing the efficacy of various interventions in OIR. However, obtaining large datasets of retinal images from OIR is costly and may require collaboration between established OIR laboratories.[15] There remains a need for publicly available datasets for OIR, which has the potential to accelerate the development of future artificial intelligence (AI) algorithms and further stimulate OIR research.[18]

The purpose of this article is to describe an open-source, publicly available dataset of flat-mounted retinal images and their corresponding vessel segmentations. This dataset was previously used to train a DL-based algorithm to segment major vessels from flat-mounted retinal images[16] and validate cumulative tortuosity index (CTI) as a metric of vascular tortu-osity in the OIR model. This repository is published at dx.doi.org/10.6084/m9.figshare.23690973 for public use.

Methods

Animals

OIR was induced in C57BL/6J mice (The Jackson Laboratory, Bar Harbor, ME, USA) as previously described.[3] From P7 to P12, pups and their mothers were transferred from room air to a hyperoxic (75% O_2) chamber (BioSpherix, Parish, NY, USA) where the hyperoxic environment led to VO of central retinal vasculature. Pups were returned to room air on P12 and transferred to a surrogate mother to facilitate survival. The relatively hypoxic conditions of room air result in ischemia that drives a neovascular phase of OIR beginning on P12, immediately upon removal from hyperoxia, and peaks on P17. The NV phase is characterized by the formation of pre-retinal neovascular tufts surrounding a central area of VO. By P25, the OIR phenotype spontaneously regresses toward a normal vascular architecture. Mice in normoxic experiments were C57BL/6J mice (The Jackson Laboratory) that matured in room air.

Intravitreal Injections

Intravitreal injections were performed using a 33-gauge needle (Hamilton Company, Reno, NV, USA) as previously described.[3] All injections were 0.5 µL in volume and performed on P12. File names are listed alongside treatment agent, mice age at treatment, mice age at sacrifice, and dosing are listed in Supplementary Table S1 with labels described in Supplementary Table S2. The number placed in the brackets after each of these treatments is correlated to the number provided in the labels described in Supplementary Table S2. Cells intravitreally injected into OIR mice included umbilical cord blood-derived endothelial colony forming cells (ECFCs) [3] and ECFCs lentivirally transduced with short hairpin RNA against CD44 (ECFCs-shCD44) [10]. All cells were injected at a concentration of 1×10^5 cells/µL in PBS vehicle. Cell culture methods are described in depth elsewhere.[3] Aflibercept (Eylea) was purchased from a pharmacy (McKesson Specialty Health, La Vergne, TN, USA), and eyes were injected with a volume of 0.5 µL containing either 2.5 µg/µL or 25 µg/µL [28].[19]

Different populations of extracellular vesicles (EVs) were also intravitreally injected into OIR mice. EV populations injected into OIR mice were harvested

from media conditioned by the following cell lines: ECFCs sorted for high expression of CD44 (CD44^{hi}) [6], ECFCs sorted for low expression of CD44 (CD44^{lo}) [7], HUVECs [11], and RPE [12]. In some experiments, vesicles from CD44^{hi} ECFCs (EVs^{hi}) were depleted via ultracentrifugation for 18 hours at $120,000g$ before injection [13]. EVs^{hi} were also incubated with antibodies to integrins $\alpha V \beta 3$ [17], $\beta 1$ [18], or $\alpha 5$ [19] or isotype control antibodies IgG$_{1a}$ [14], IgG$_{2a}$ [15], or IgG$_{2b}$ [16].

EVs were isolated using a protocol that used serial ultrafiltration, size exclusion chromatography, and repeat ultrafiltration to harvest vesicles from conditioned media. Details of these isolation protocols are described elsewhere.[3] In brief, serum-free XFM (10 mL/T75 flask) was conditioned for 48 hours by ECFCs seeded at a density of 1.2×10^6 cells/T75 flask (07-202-000; Thermo Fisher Scientific, Waltham, MA, USA). After centrifugation at $300\ g$ for five minutes (Alegra 6KR, ARIES Smart Balance Rotor; Beckman Coulter, Inc., Southfield, MI, USA) to remove cell debris, the supernatant was vacuum filtered (0.22 µm, 430320; Corning Inc., Corning, NY, USA) before being loaded into an Amicon Ultra-15 Centrifugal Filter Unit with an Ultracel-10 membrane (UFC901024, MWCO = 10 kDa; Merck Millipore, Burlington, MA, USA). The supernatant was ultrafiltered via centrifugation at $4000\ g$ for approximately 45 minutes (Beckman GS-6R, GH-3.8 swing bucket rotor; Beckman Coulter, Inc.) to concentrate CM to 1 mL. This concentrated sample was subjected to SEC as previously described with modifications.[3] The SEC column was a 10 mL plastic syringe (309604; BD Bioscience, Franklin Lakes, NJ, USA) packed with nylon stocking (20 denier, H&M, Stockholm, Sweden) that was loaded with 10 mL sepharose CL-2B (17014001; GE-Healthcare, Chicago, IL, USA), which was washed three times beforehand with elution buffer (PBS with 0.32% trisodium citrate, pH 7.4, 0.22 µm vacuum filtered). Once the column ran dry, the UF-concentrated CM was loaded. Once all CM entered the column, 20 mL of elution buffer was slowly added to not agitate the bears, and eluate was collected in approximately 40 sequential elution fractions (EFs) of 0.5 mL each. A Pierce BCA protein assay assay (23225; Thermo Fisher Scientific) was used to measure soluble protein of each EF according to the manufacturer's instructions. Protein began eluting between fraction 8 and 12. EFs before protein detection were pooled and concentrated using an Amicon Ultra-4 Centrifugal Filter Unit with an Ultracel-10 membrane (UFC801024, MWCO = 10 kDa; Merck Millipore) that was spun in a centrifuge at $4000\ g$ for approximately 45 minutes. This protocol has been demon-strated to produce an EV-rich, soluble protein–poor EV sample.[3] Sample concentrations were measured with Nanoparticle Tracking Analysis and aliquoted for experiments fresh or after storage at $-80°C$. One experiment was performed by injecting EVs that were harvested using ultracentrifugation on media conditioned by CD44^{hi} [4] and CD44^{lo} ECFCs [5]. EVs harvested using differential ultracentrifugation were isolated using a Beckman Coulter Optima L-80 XP ultracentrifuge as previously described.[20]

Mechanistic studies injected EVs harvested from CD44^{hi} ECFCs with individual or combinatorial knockdown of their expression of microRNAs (miR) by using miRCURY LNA miRNA Power Inhibitors as previously described.[3] Transfection efficiency was measured as the average percentage of DAPI[+]/GFP^{+} cells in five sample confocal images of cells fixed in 4% formaldehyde for 20 minutes. Transduction efficiencies were measured on RT-qPCR. OIR mice were also injected with populations of EVs harvested from CD44^{hi} ECFCs with individual knockdown miR-23a-3p [23], as well as with combinatory knockdown of both miR-216a-3p and miR-503-5p [24] and separately with EVs harvested from CD44^{hi} ECFCs with knocked down expression of miR-7-5p, miR-23a-3p, miR-216a-3p, and miR-503-5p [25]. Combinations of microRNA mimics (ThermoFisher, St. Louis, MO, USA) of both miR-216a-3p and miR-503-5p [21] and separately a combination of all miR-7-5p, miR-23a-3p, miR-216a-3p, and miR-503-5p mimics [22] were also injected alongside scramble miR controls [20].

Additional controls included PBS vehicle [2], media conditioned by CD44^{hi} cells [26], media conditioned by CD44^{lo} cells [27], as well as non-conditioned ECFC media [8] (XFM, STEMCELL Technologies, 0800) and non-conditioned XFM subject to the EV isolation protocol [9]. Some eyes were also untreated [1].

Retinal Flat-Mounts, Immunostaining, and Imaging

Preparation of retinal flat-mounts was performed as previously described.[3] Enucleated eyes were fixed in 4% paraformaldehyde at 4°C for one hour. The anterior capsule was removed, and the nuclei and cortex of the lens were dissected. Then the retina was separated from the choroid and sclera and cleaned of adherent vitreous using fine brushes before being cut into 4 leaflets. To fluorescently label vasculature, retinas were incubated in PBS with $Ca^{2+}Mg^{2+}$ with 10 µg of GS-IB4 (I21412; Thermo Fisher Scientific). Retinas were washed four times in PBS for 10 minutes before mounting with SlowFade Gold Antifade Mountant medium (S36937; Thermo Fisher Scientific). Retinas were imaged using

a Zeiss 710 confocal laser-scanning microscope with ZEN 2010 software (Zeiss, Oberkochen, Germany). All retinal images contained the entire retinal flat mount and were generated by stitching 5×5 individual images using Zeiss software.

Study Approval

Approval for all experimental procedures using animals was provided by Scripps Research Animal Care and Use Committee. Experiments were performed in accordance with the NIH Guide for the Care and Use of Laboratory Animals (National Academies Press, 2011). Adult donors of umbilical cord blood provided informed consent before sample collection in accordance with the Declaration of Helsinki. Protocols were approved by the Institutional Review Board at Scripps Research and Scripps Memorial Hospital, La Jolla, CA, USA.

Data Summary

Overall, 1170 eyes were included (Table). These images were selected from various previously published articles, as well as from the OIRSeg dataset.[3,4,16,19,21] Images were subject to a rigorous cross-validation process described in "Technical Validation." Our training and held-out test set consisted of 1084 images of normoxic and OIR mice sacrificed P12, P17, and P25. Other datasets included 50 images of OIR mice sacrificed at an unknown age taken from an external dataset named OIRSeg. Thirty-six images of OIR P17 retinas were included from Xin et al.,[19] where 18 images were from eyes given aflibercept or IgG Control. The majority of images in the training and held out test-set were subject to the OIR model and sacrificed at P17. Example images of raw flat-mounted images and their corresponding manual vessel segmentations are shown in Figure 1.

This dataset is publicly available at dx.doi.org/10.6084/m9.figshare.23690973. The dataset has been uploaded as a zip file with accompanying metadata
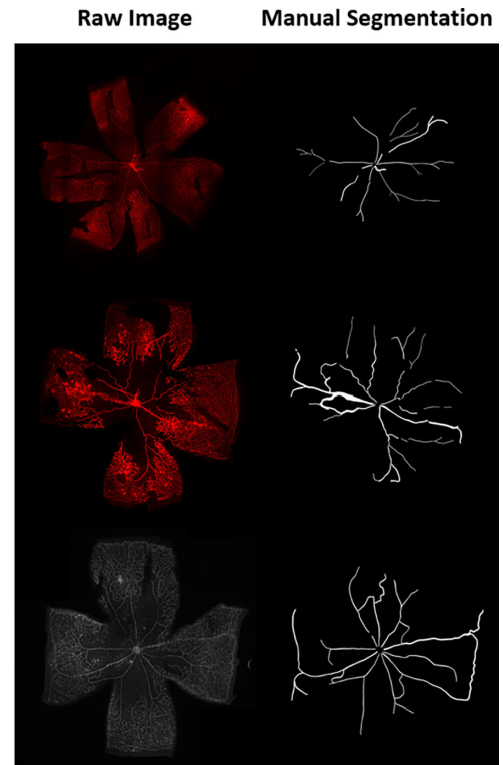
Figure 1. Representative raw flat-mounted retinal images and their corresponding manual segmentations from normoxic mice, the OIRSeg dataset, and eyes treated by aflibercept.

including a data dictionary containing the image names, paths, age at sacrifice, normoxia (NOX) versus OIR labels, and any experiments performed on the mice if applicable. A legend defining the experiments performed is also provided in Supplementary Table S2. This dataset is available under the Creative Commons Attribution 4.0 International license. To promote data transparency, a HealthSheet is provided detailing the use cases of our dataset and terms of data collection, among other details (Supplemental Materials).

The 1084 images in the training and held-out testing sets are sorted within the "Age-Matched Controls" folder, with subfolders labeled P12 NOX, P12 OIR, P17 NOX, P17 OIR, P25 NOX, and P25 OIR. These folders are labeled by the age the mice were sacrificed (P12, P17, P25) and their NOX versus OIR experimen-

Table. Distribution of Images in the Training, Internal, Held-out, and External Test Sets by Age at Sacrifice

Dataset	P12 NOX	P12 OIR	P17 NOX	P17 OIR	P25 NOX	P25 OIR	Total
Training Set	38	27	28	815	45	31	984
Held-out Test Set	4	3	3	83	4	3	100
External Test Set (OIRSeg)	Unknown	Unknown	Unknown	Unknown	Unknown	Unknown	50
Aflibercept vs. IgG Control[19]	0	0	0	36	0	0	36

Images from the OIRSeg dataset did not have age data available.
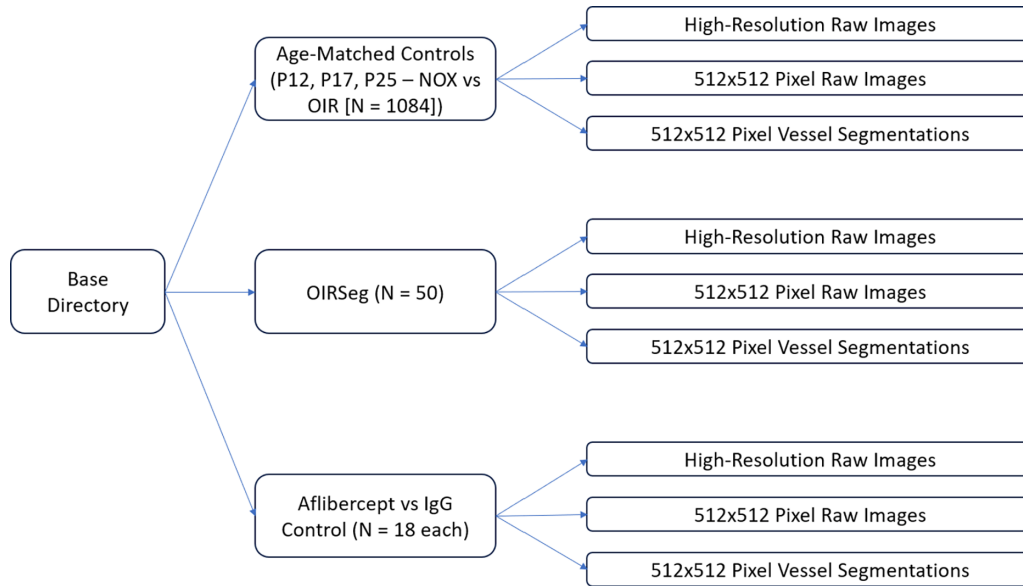
Figure 2. File directory structure of the published dataset, available online at dx.doi.org/10.6084/m9.figshare.23690973.

tal groups. The 50 images from the OIRSeg are located in the "OIRSeg" folder. The "Afllipercept vs IgG Control" contains two subfolders, "Aflibercept" and "IgG Control" containing 18 images each. All subfolders in this dataset contain three folders with the high-resolution raw images, 512×512 pixel raw images, and 512×512 pixel vessel segmentations. A schematic of the folder organization is shown in Figure 2.

Technical Validation

All images were produced using a previously published protocol for OIR.[3] Images included in this dataset underwent manual review by an expert ophthalmologist (JSC) for image quality and vessel fidelity.

Manual vessel segmentations were generated by a cross-validation process previously described.[21] In brief, four graders (JSC, HKR, KBL, and JM) initially segmented 10 random images manually and compared manual vessel segmentations subjectively. Disagreement was resolved by discussion until subjective consensus on segmentation methodology was achieved. Manual vessel segmentations were then compared objectively using the Dice coefficient, with statistical significance evaluated using one-way analysis of variance. Comparison of the Dice coefficient for all six combinations of four graders (0.79 ± 0.13, 0.58 ± 0.27, 0.63 ± 0.25, 0.61 ± 0.1, 0.61 ± 0.21, and 0.57 ± 0.24) demonstrated no significant differences in vascular segmentation ($P = 0.24$). This suggested

that manual segmentation divided among four graders was a reliable method segment vessels in this dataset. All images included in this dataset were segmented by an author that participated in this cross-validation process.

Discussion

This dataset is the first large open-sourced dataset of retinal flat-mounts from OIR and NOX mice. Most of these flat-mounted retinas were from OIR mice at P17, which is the most commonly used endpoint to quantify outcome metrics in the model. The dataset also provides mice retinas at P12, immediately on return to room air, and P25, the time point at which retinal blood vessels spontaneously regress toward more normal vascular architecture. In addition, the repository consists of age-matched controls consisting of retinas from normoxic wild-type mice killed at the corresponding postnatal days (P12, P17, and P25).

Prior machine learning models have been developed to quantify outcome parameters that characterize OIR disease severity, but only recently was the first artificial intelligence (AI)-based model, OIRseg, generated to allow for the standardized semi-automated quantification of such metrics using deep learning. Trained on a dataset similar to that published in this manuscript, OIRseg rapidly quantifies NV and VO in a more reproducible, scalable, and objective assessment of OIR severity and treatment response.[15]

Another recently published AI-based model provided an automated method to measure vascular tortuosity in OIR mice.[16,21] These studies generated a cumulative tortuosity index (CTI) for retinal flat-mount images by adapting a computer-based image analysis algorithm called iROP-Assist that is publicly available and has been validated on fundus images in human ROP. The iROP-Assist algorithm was initially used on manual segmentation of vasculature in images of retinal flat-mounts.[21] The process of segmentation has been automated by the development of a generative adversarial network using the same dataset.[16] Retinal vessel tortuosity characterized at time points of pathophysiological significance in the OIR model correlated with disease severity.[21] Therapeutic interventions used in the treatment of ROP reduced retinal vascular tortuosity in OIR mice. Together these data used big data to generate an AI model to standardize and automate the quantification of vascular tortuosity, which on full characterization may be another useful biomarker of disease severity in OIR, as well as a novel outcome measurement in experiments aimed at testing new therapeutic strategies in this in vivo model of ischemic retinopathy.

This AI model was trained using the current manuscript's dataset. Thus there are several advantages of publishing this dataset. First, the dataset could be used to train or augment AI models used in OIR. Future work may append this data to training sets of existing AI models to improve the quality of current algorithms, such as the quantification of NV or VO by OIRseg. The dataset is also large enough to independently discover, validate, and characterize novel biomarkers, such as vessel dilation. Combined with datasets from other institutions, this open dataset could also be useful in increasing the performance and generalizability of AI models. Second, conducting experiments using the OIR model is a time-consuming effort, requiring expertise and significant costs. Use of publicly available big data to develop new AI circumvents this labor and expense. Third, the dataset contains flat-mounted retinas of normoxic mice at P12, P17, and P25. These served as age-matched controls in our study validating vascular tortuosity and can once again be used as an age-matched control group for future work aimed at validating novel features of retinas from OIR or other models at similar time points.

There are limitations to this dataset that should be noted. Although use of this big dataset saves resources, readers are cautioned to substitute our control groups as their own. An in vivo model, OIR mice are notably variable. It remains best practice to conduct experiments in OIR mice by comparing the effects in one treated eye to the contralateral eye injected with appropriate controls.

This publicly available dataset may serve as a source of raw data for future efforts integrating AI into basic and translational research. Our hope is that this dataset encourages other researchers to publish big datasets across animal models to save resources and facilitate such research.

References

1. Smith LE, Wesolowski E, McLellan A, et al. Oxygen-induced retinopathy in the mouse. *Invest Ophthalmol Vis Sci*. 1994;35:101–111.
2. Scott A, Fruttiger M. Oxygen-induced retinopathy: a model for vascular pathology in the retina. *Eye*. 2010;24:416–421.
3. Marra KV, Aguilar E, Guoqin W, et al. Bioactive extracellular vesicles from a subset of endothelial progenitor cells rescue retinal ischemia and neurodegeneration. *JCI Insight*. 2022;7(12).

4. Bucher F, Aguilar E, Marra KV, et al. CNTF prevents development of outer retinal neovascularization through upregulation of CxCl10. *Invest Ophthalmol Vis Sci*. 2020;61(10):20.

5. Dalvin LA, Hartnett ME, Bretz CA, et al. Stanniocalcin-1 is a modifier of oxygen-induced retinopathy severity. *Curr Eye Res*. 2020;45:46–51.

6. Albert DM, Scheef EA, Wang S, et al. Calcitriol is a potent inhibitor of retinal neovascularization. *Invest Ophthalmol Vis Sci*. 2007;48:2327–2334.

7. Rojo Arias JE, Englmaier VE, Jászai J. VEGF-trap modulates retinal inflammation in the murine oxygen-induced retinopathy (OIR) model. *Biomedicines*. 2022;10:201.

8. Tokunaga CC, Mitton KP, Dailey W, et al. Effects of anti-VEGF treatment on the recovery of the developing retina following oxygen-induced retinopathy. *Invest Ophthalmol Vis Sci*. 2014;55:1884–1892.

9. Li Calzi S, Shaw LC, Moldovan L, et al. Progenitor cell combination normalizes retinal vascular development in the oxygen-induced retinopathy (OIR) model. *JCI Insight*. 2019;4(21).

10. Becker S, Wang H, Yu B, et al. Protective effect of maternal uteroplacental insufficiency on oxygen-induced retinopathy in offspring: removing bias of premature birth. *Sci Rep*. 2017;7:42301.

11. Kvarik T, Reglodi D, Werling D, et al. The protective effects of endogenous PACAP in oxygen-induced retinopathy. *J Mol Neurosci*. 2021;71:2546–2557.

12. Zhang H, Sun N, Liang H, Xiao X, Liu X, Wang Y. The protective effect of 17 beta-estradiol on oxygen-induced retinopathy and its relation with the changes of malondialdehyde. *J Biomed Res*. 2010;24:138–144.

13. Usui-Ouchi A, Eade K, Giles S, et al. Deletion of TGFβ signal in activated microglia prolongs hypoxia-induced retinal neovascularization enhancing Igf1 expression and retinal leukostasis. *Glia*. 2022;70:1762–1776.

14. Simmons MA, Cheng AV, Becker S, Gerkin RD, Hartnett ME. Automatic analysis of the retinal avascular area in the rat oxygen-induced retinopathy model. *Mol Vis*. 2018;24:767–777.

15. Xiao S, Bucher F, Wu Y, et al. Fully automated, deep learning segmentation of oxygen-induced retinopathy images. *JCI Insight*. 2017;2(24):e97585.

16. Chen JS, Marra KV, Robles-Holmes HK, et al. Applications of deep learning: automated assessment of vascular tortuosity in mouse models of oxygen-induced retinopathy. *Ophthalmology Science*. 2023;4(1):100338.

17. Zingman I, Zippel N, Birk G, et al. Deep learning-based detection of endothelial tip cells in the oxygen-induced retinopathy model. *Toxicol Pathol*. 2021;49:862–871.

18. Zarbin MA, Lee AY, Keane PA, Chiang MF. Data science in translational vision science and technology. *Transl Vis Sci Technol*. 2021;10(8):20.

19. Xin H, Biswas N, Li P, et al. Heparin-binding VEGFR1 variants as long-acting VEGF inhibitors for treatment of intraocular neovascular disorders. *Proc Natl Acad Sci USA*. 2021;118(21):e1921252118.

20. Nordin JZ, Lee Y, Vader P, et al. Ultrafiltration with size-exclusion liquid chromatography for high yield isolation of extracellular vesicles preserving intact biophysical and functional properties. *Nanomedicine*. 2015;11:879–883.

21. Marra KV, Chen JS, Robles-Holmes HK, et al. Vascular tortuosity quantification as an outcome metric of the oxygen-induced retinopathy model of ischemic retinopathy. bioRxiv. 2022:2022.10.02.510568.

translational vision science & technology